JOURNAL OF GEOPHYSICAL RESEARCH, VOL. 115, A07222, doi:10.1029/2009JA015166, 2010

Substorm triggering by new plasma intrusion: THEMIS all-sky imager observations

Y. Nishimura,[1,2] L. Lyons,[1] S. Zou,[1,3] V. Angelopoulos,[4] and S. Mende[5]

Received 4 December 2009; revised 16 March 2010; accepted 1 April 2010; published 27 July 2010.

[1] A critical, long-standing problem in substorm research is identification of the sequence of events leading to substorm auroral onset. Based on event and statistical analysis of THEMIS all-sky imager data, we show that there is a distinct and repeatable sequence of events leading to onset, the sequence having similarities to and important differences from previous ideas. The sequence is initiated by a poleward boundary intensification (PBI) and followed by a north-south (N-S) arc moving equatorward toward the onset latitude. Because of the linkage of fast magnetotail flows to PBIs and to N-S auroras, the results indicate that onset is preceded by enhanced earthward plasma flows associated with enhanced reconnection near the pre-existing open-closed field line boundary. The flows carry new plasma from the open field line region to the plasma sheet. The auroral observations indicate that Earthward-transport of the new plasma leads to a near-Earth instability and auroral breakup ~5.5 min after PBI formation. Our observations also indicate the importance of region 2 magnetosphere-ionosphere electrodynamic coupling, which may play an important role in the motion of pre-onset auroral forms and determining the local times of onsets. Furthermore, we find motion of the pre-onset auroral forms around the Harang reversal and along the growth phase arc, reflecting a well-developed region 2 current system within the duskside convection cell, and also a high probability of diffuse-appearing aurora occurrence near the onset latitude, indicating high plasma pressure along these inner plasma sheet field lines, which would drive large region 2 currents.

Citation: Nishimura, Y., L. Lyons, S. Zou, V. Angelopoulos, and S. Mende (2010), Substorm triggering by new plasma intrusion: THEMIS all-sky imager observations, *J. Geophys. Res.*, *115*, A07222, doi:10.1029/2009JA015166.

1. Introduction

[2] Substorms are a dramatic disturbance of the global magnetosphere-ionosphere system that release large amounts of solar wind energy accumulated in the magnetotail [e.g., *Rostoker et al.*, 1980] and are associated with auroral activations [*Akasofu*, 1964]. Although substorms have been studied extensively from the ground and in space for the past 40 years, the sequence of events leading to substorm onset has remained elusive and been a key subject of debate [*McPherron*, 1979; *Akasofu*, 2004]. Substorm onset, which can be identified by its ionospheric manifestation (an auroral onset), starts along an arc near the equatorward boundary of the auroral oval and likely maps along magnetic field lines toward the near-Earth portion of the electron plasma sheet [*Samson et al.*, 1992]. The main debate has been whether substorm onset is triggered by magnetic reconnection in the mid-tail plasma sheet (~20–30 *RE*, downtail from the Earth) or by a current disruption process along the near-Earth plasma sheet field lines (~10 *RE* downtail) [*Angelopoulos*, 2008].

[3] Recent THEMIS spacecraft observations during radially aligned spacecraft configurations in the magnetotail have given evidence that magnetotail reconnection occurs prior to substorm onset [*Angelopoulos et al.*, 2008; *Lin et al.*, 2009]. Mid-tail reconnection is expected to lead to onset by driving longitudinally localized flows from the reconnection region toward the near-Earth onset region [*Birn et al.*, 1999]. Although a statistical study using Geotail spacecraft observations shows evidence for enhancements of the plasma flow in the plasma sheet shortly before auroral onset [*Miyashita et al.*, 2009], onsets in this study were determined from global auroral images from space, which cannot reliably detect the initial brightening of a thin breakup auroral arc. On the other hand, localized plasma sheet flows are known to be related to auroral activity. Specifically, poleward boundary intensifications (PBIs) have been related to enhanced flows that carry plasma across the nightside separatrix [*de la Beaujardière et al.*,

[1]Department of Atmospheric and Ocean Sciences, University of California, Los Angeles, California, USA.
[2]Solar-Terrestrial Environment Laboratory, Nagoya University, Nagoya, Japan.
[3]Department of Atmospheric, Oceanic and Space Sciences, University of Michigan, Ann Arbor, Michigan, USA.
[4]Institute of Geophysics and Planetary Physics, University of California, Los Angeles, California, USA.
[5]Space Science Laboratory, University of California, Berkeley, California, USA.

0148-0227/10/2009JA015166

1994] into the plasma sheet [*Lyons et al.*, 1999]. Some PBIs develop into equatorward-moving auroral arcs with roughly north-south (N-S) orientations (also called "auroral streamers"), which have been related to channels of enhanced earthward flows within the plasma sheet [*Rostoker et al.*, 1987; *Sergeev et al.*, 1999, 2000; *Nakamura et al.*, 2001; *Zesta et al.*, 2002; *Henderson et al.*, 2002]. Thus, if mid-tail reconnection were to lead to onset, the flows coming from the reconnection location to the near-Earth onset should lead to N-S aurora moving equatorward toward onset latitudes. *Elphinstone et al.* [1995] suggested that N-S arcs may precede some substorm onsets and recently *Kepko et al.* [2009] noted an equatorial moving diffuse aurora feature prior to onset for one event, suggesting it might be related to mid-tail reconnection. However, neither of these features has not been verified as a common pre-cursor to onset. This lends support for a near-Earth instability process leading to onset, in order to explain auroral onset occurring near the equatorward boundary of the auroral oval [*Lui and Burrows*, 1978; *Roux et al.*, 1991; *Lui* 1991; *Samson et al.*, 1992; *Donovan et al.*, 2008]. In the present paper, we use auroral observations from the THEMIS ground array of all-sky imagers (ASIs) [*Mende et al.*, 2008], which have high spatial and temporal resolutions as well as broad latitudinal and longitudinal coverage. We show that there is a distinct and repeatable sequence of events leading to onset, the sequence having similarities, but also important differences, from the above ideas for substorm onset.

[4] Our analysis of pre-onset aurora also reveals important connections to the flow pattern and plasma distributions previously associated with the electrodynamic magnetosphere-ionosphere coupling of the region 2 current system. Connections between substorm and region 2 electrodynamics have been found previously. These connections include simultaneous radar and optical observations, which have shown that auroral onsets tend to occur close to or equatorward of the Harang flow shear [*Baumjohann et al.*, 1981; *Bristow et al.*, 2003; *Zou et al.*, 2009a, 2009b], which results from region 2 magnetosphere-ionosphere coupling and substantially distorts the duskside convection cell [*Erickson et al.*, 1991; *Gkioulidou et al.*, 2009]. In addition, enhanced subauroral polarization streams (SAPS) have been found to be closely related to substorm onset and expansion phase development [*Lyons et al.*, 2009; *Zou et al.*, 2009a, 2009b]. Driven by region 2 field-aligned currents (FACs), SAPS are associated with the region of approximately pure proton precipitation that lies equatorward of the electron plasma sheet, and they form duskward flows equatorward of the center of the Harang reversal. These observations indicate that existence of a well-developed region 2 current system is a pre-condition for substorm onset in the pre-midnight sector. Since plasma convection is substantially affected by the Harang flow shear, examination of the motion of pre-onset auroras in relation to the Harang flow shear offers the opportunity to evaluate how the guiding of any pre-onset flow enhancements by the background flow influences the occurrence of onset and its location relative to the duskside and morningside convection cells.

[5] The THEMIS ASI array allows detection of faint, localized aurora that might precede substorm onset. Taking advantage of this observational capability, we perform event analyses and occurrence statistics of various timing sequence features that we have found to lead to substorm onset. We also evaluate the time delays between subsequent phenomena and the coupling of the sequence features to the flow pattern associated with the region 2 magnetosphere-ionosphere coupling. Our analysis shows that the sequence of events leading to onset is initiated by a PBI and followed by an N-S arc moving equatorward toward the onset latitude. Because of the linkage of fast magnetotail flows to PBIs and to N-S auroras, the results lead us to propose that onset is preceded by enhanced earthward plasma flows, which first carry plasma from the open field line region to the plasma sheet in association with enhanced reconnection near the pre-existing open-closed field line boundary and then transport plasma toward the near-Earth region. We also provide evidence that region 2 magnetosphere-ionosphere coupling plays an important role in the motion of pre-onset auroral forms and the local times of onsets. Note that in the companion paper [*Lyons et al.*, 2010], we use ground incoherent scatter radar measurements to look for direct evidence for the ionospheric flows inferred from our auroral observations.

2. Case Study

[6] In this section, we present three examples illustrating the sequence of events in the ASI that we have repeatedly found to lead to onset. The events selected also illustrate how the guidance by the pre-existing convection pattern appears to influence the magnetic local time (MLT) of onset. Here onset refers to the initiation of substantial intensification of an auroral arc near the equatorward boundary followed by a poleward expansion lasting more than 3 min [*Akasofu*, 1964; *Angelopoulos et al.*, 2008] together with enhancements of the westward electrojet identified by ground magnetometers.

2.1. The 29 February 2008 Auroral Breakup

[7] Figures 1 and 2 present keograms and a sequence of images from four ASIs during a substorm auroral onset at 8:22 UT on 29 February 2008 (see Movie S1 for the entire image sequence).[1] During the growth phase, as shown in Figure 2a, a broad growth phase arc extended azimuthally near the equatorward boundary of the auroral oval at ~64° magnetic latitude (MLAT). This aurora persisted for several hours due to the long southward IMF period. The poleward boundary of the auroral oval was located at ~69° MLAT roughly parallel to the growth phase arc. A PBI initiated at 08:14:48 UT, 7 min prior to the auroral onset. This PBI is identified in Figure 2b as a brighter spot at the poleward boundary with a narrow longitudinal width (~0.3 h). An N-S arc with a ~0.1 h width then extended equatorward from the PBI (Figure 2c) tilting toward the west. Soon after the N-S arc reached the equatorward portion of the auroral oval, a pseudo-breakup occurred near the western edge of the ATHA imager field-of-views (FOVs) in Figure 2d. The N-S arc can be seen to have reached very close to the growth phase arc, but the narrow width and weakness of the leading edge of the N-S arc, in addition to the somewhat hazy

[1] Auxiliary material data set are available at ftp://ftp.agu.org/apend/ja/2009ja015166. Other auxiliary files are available in the HTML.

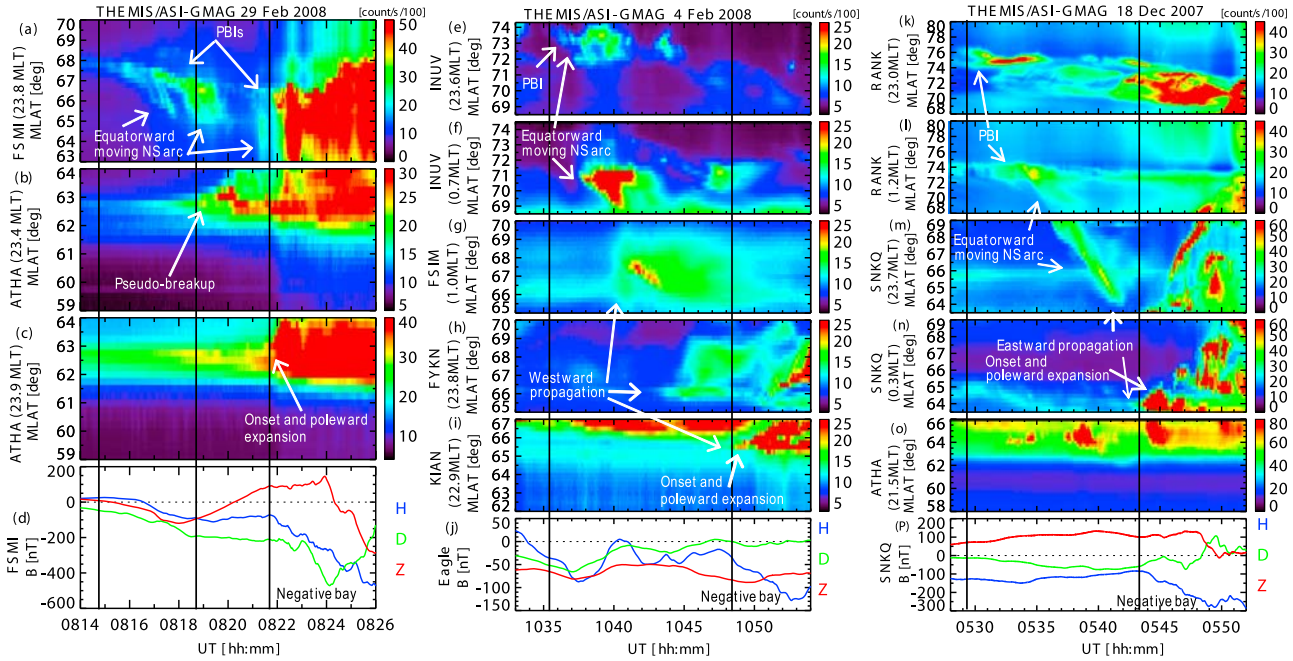

Figure 1. Keograms and magnetograms of (a–d) 29 February 2008, (e–j) 4 February 2008 and (k–p) 12 December 2007 onsets corresponding to ASI data shown in Figures 2–4. MLTs at the central times of each keogram are shown in the labels. Light-contaminated area in panel (i) is masked in gray.

conditions at ATHA, made it difficult to identify if the N-S arc contacted the growth phase arc or not. A further PBI occurred at 08:21:00 UT (Figure 2e), and a bright patch originating from the poleward boundary moved equatorward along the pre-existing N-S arc (Figure 2f). An auroral onset started at the meridian of the N-S arc reaching the equatorward portion of the auroral oval at 22.8 MLT almost immediately after the bright N-S arc reached the equatorward growth phase arc at 08:21:48 UT (Figure 2g), which was followed by poleward expansion of auroral activity (Figure 2h). While skies were cloudy west of the imager FOVs in Figure 2, this onset was near the center of the ATHA FOV and there is no evidence for an onset west of the ATHA FOV in ground magnetometers.

[8] Keograms at three different magnetic meridians and magnetometer data near the onset location (FSMI) shown in Figures 1a–1d also demonstrate the sequence of the pre-onset auroral form in relation to substorm onset. The onset (third vertical line) was marked by substantial auroral intensification starting near the equatorward boundary of the auroral oval followed by poleward expansion, seen near 23.9 MLT in Figure 1c. Onset was also accompanied by enhancement of the westward electrojet, as inferred from an abrupt decrease in the ground magnetic H component (Figure 1d). The second vertical line indicates initiation of the pseudo-breakup (Figure 1b) seen in Figure 2d, which occurred 0.5 MLT to the west of the full onset. PBIs and ensuing equatorward-moving auroral intensifications from the poleward boundary, the latter two leading to the pseudo-breakup and the full onset, are identified in Figure 1a. The slight intensification of the auroral arc ~45 s before full onset in Figure 1c reflects some azimuthal spreading of the incoming N-S aurora after it reached the equatorward portion of the auroral oval. There was no other notable auroral activity for the preceding hour; however, gradual ground perturbations prior to onset occurred further to the west (not shown), which are the normal response to enhanced convection during the growth phase.

2.2. The 4 February 2008 Auroral Breakup

[9] The N-S arc shown in Figures 2e–2g has only small curvature with respect to the magnetic meridian. The onset occurred very close to the meridian of the N-S arc reaching the equatorward portion of the auroral oval, indicating an approximately radial plasma transport through the magnetotail toward the onset location in the near-Earth plasma sheet. However, as will be shown here and in the statistical study in the next section, pre-onset arcs tend to be highly tilted with respect to the meridional direction and to reach onset location from the east. Moreover, auroral onset does not often occur at the meridian of the N-S arc reaching the equatorward portion of the auroral oval, but the pre-onset auroral form turns azimuthally toward the onset location, which is frequently to the west of the N-S arc.

[10] Figure 3 presents a sequence of selected images from four ASIs during a substorm auroral onset that occurred at 10:48 UT on 4 February 2008 in the Alaskan sector (See Movie S2 for the entire image sequence). Initially (Figure 3a), a faint, pre-existing growth phase arc extended azimuthally at ~66° MLAT. A bright auroral structure in the premidnight sector in the FOV of the FYKN imager, marked "Harang aurora," rotated clockwise as clearly identified in the movie: the poleward and equatorward portions moved eastward and westward, respectively, with equatorward motion at the eastern edge of the structure. Based on the relationship between flows and auroral features discussed above, this

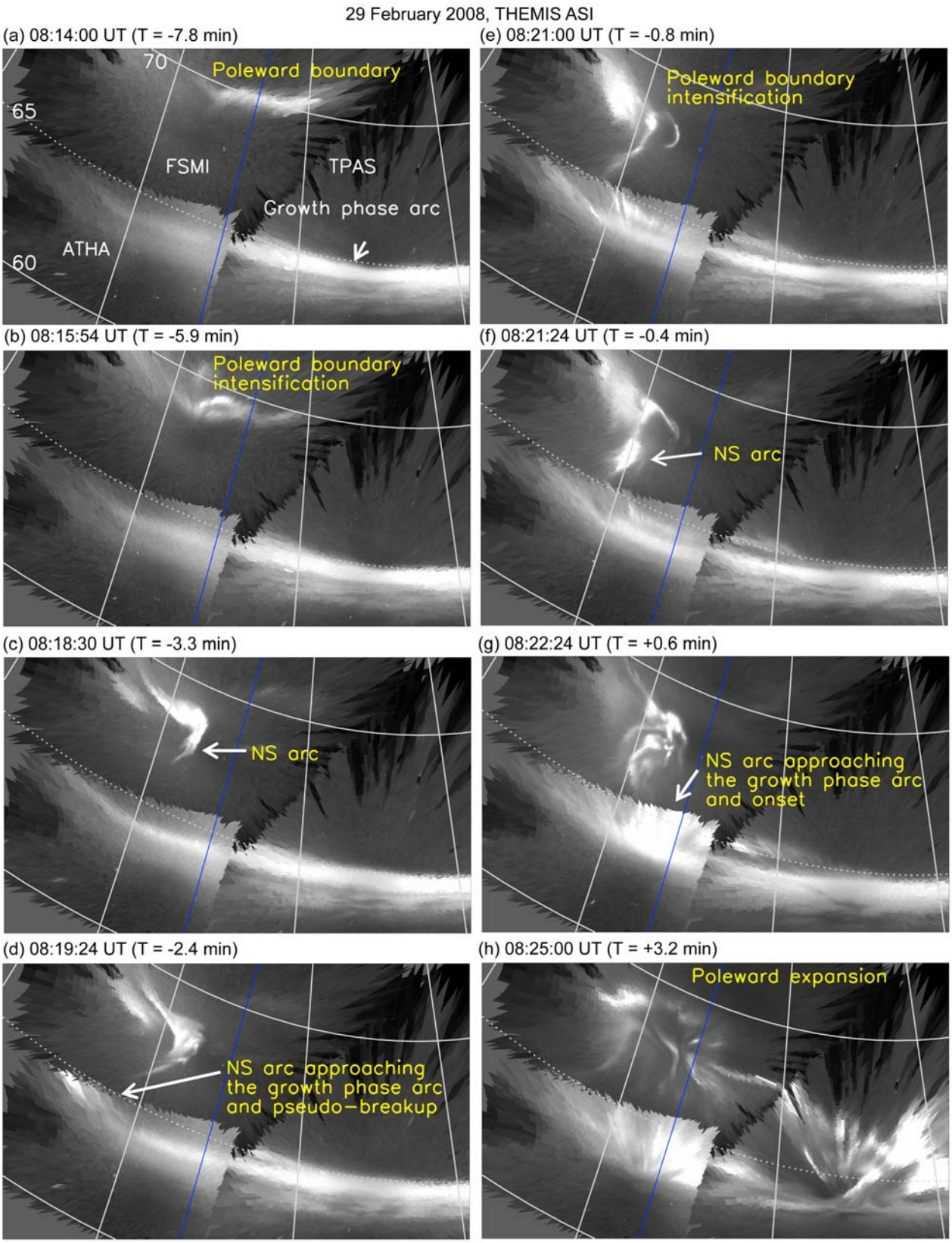

Figure 2. THEMIS ASI data during an auroral onset on 29 February 2008. ASIs used are RANK (65.13° MLAT and 253.47° MLON), FSMI (67.24° MLAT and 266.14° MLON), ATHA (71.23° MLAT and 275.09° MLON), TPAS (63.66° MLAT and 278.14° MLON). White lines are isocontours of magnetic latitude (every 10° in solid lines) and longitude (every 15°). The blue line in each plot is the magnetic midnight meridian. The onset occurred at 08:21:48 UT. The entire sequence is shown in Movie S1.

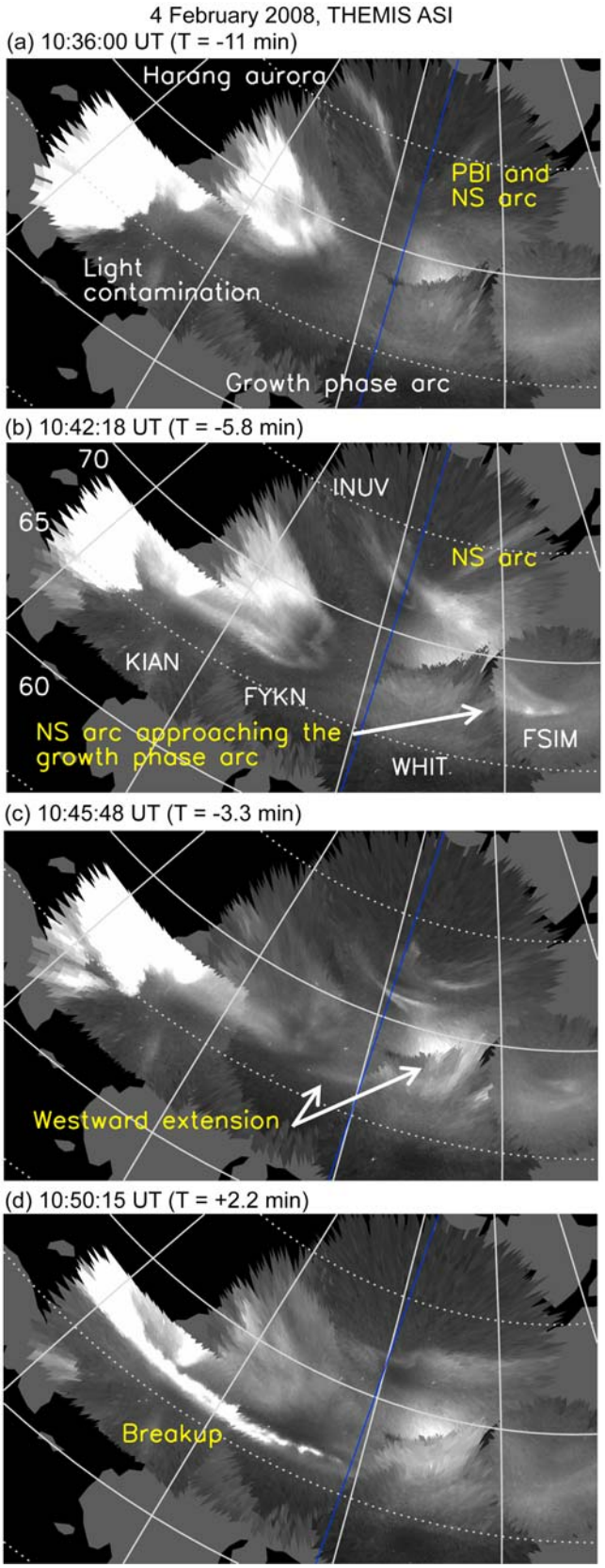

auroral motion is as expected from flows around the Harang reversal, and it is observed near the expected location of the Harang reversal within the duskside ionospheric convection cell.

[11] A PBI that initiated at ~76° MLAT at 10:35:24 UT, 12.7 min prior to auroral onset, is identified in Figure 3a as a faint auroral form in the poleward portion of the INUV imager FOV. An N-S arc extending from the PBI drifted equatorward and eastward and reached the equatorward portion of the auroral oval in the FOV of the FSIM imager ~6 min prior to auroral onset (Figure 3b). Onset did not occur at this point, but the N-S arc then turned into an east-west (E-W) oriented enhancement and continued moving westward along the pre-existing growth phase arc (Figure 3c). Finally, auroral onset started near the boundary of the KIAN and FYKN imagers FOV's (~22.9 MLT) at 10:48:06 UT, immediately after the E-W auroral enhancement reached near the onset location. The auroral onset can be seen clearly in Figure 3d (images taken 2.2 min after onset).

[12] The time evolution of the pre-onset auroral form can also be identified in keograms, as shown in Figures 1e–1i. The onset (second vertical line) is characterized by substantial auroral intensification followed by a small poleward expansion observed within the KIAN imager FOV (Figure 1i) and a weak enhancement of the westward electrojet (Figure 1j). The equatorward and eastward motion of the pre-onset auroral form seen in Figures 3a and 3b appears as a luminosity enhancement first seen at ~23.6 MLT in Figure 1e and then at ~0.7 MLT in Figure 1i. The westward-moving auroral enhancement along the pre-existing growth phase arc, which occurred after the N-S arc reached the equatorward portion of the auroral oval, can be seen at ~66° MLAT in Figures 1g, 1h and 1i. The onset occurred when the enhancement reached the meridian of Figure 1i.

[13] The equatorward motion of the N-S arc and the subsequent westward motion of the E-W arc have the same polarity of rotation as the Harang aurora. This indicates that motion of the pre-onset (substorm precursor) auroral form was organized by the two-cell ionospheric convection developed during the growth phase. As in many of our events, an N-S arc formed in the dusk convection cell at the poleward boundary of the auroral oval and then moved equatorward and eastward around the poleward portion of the Harang aurora. It then turned westward and continued moving around the equatorward portion of the flow shear within the dusk convection cell leading to onset in the premidnight sector.

[14] We emphasize that the pre-onset auroral form did not move equatorward along the onset magnetic meridian, but instead approached the onset location from the east. The N-S arc reached the growth phase arc ~2 MLT to the east of the onset location and subsequently approached the onset

Figure 3. THEMIS ASI data from Alaskan sector during an auroral onset on 4 February 2008. The format is same as Figure 2. ASIs used are KIAN (65.13° MLAT and 253.47° MLON), FYKN (67.24° MLAT and 266.14° MLON), INUV (71.23° MLAT and 275.09° MLON), WHIT (63.66° MLAT and 278.14° MLON) and FSIM (67.30° MLAT and 293.85° MLON). The onset occurred at 10:48:06 UT. The whole sequence is shown in Movie S2.

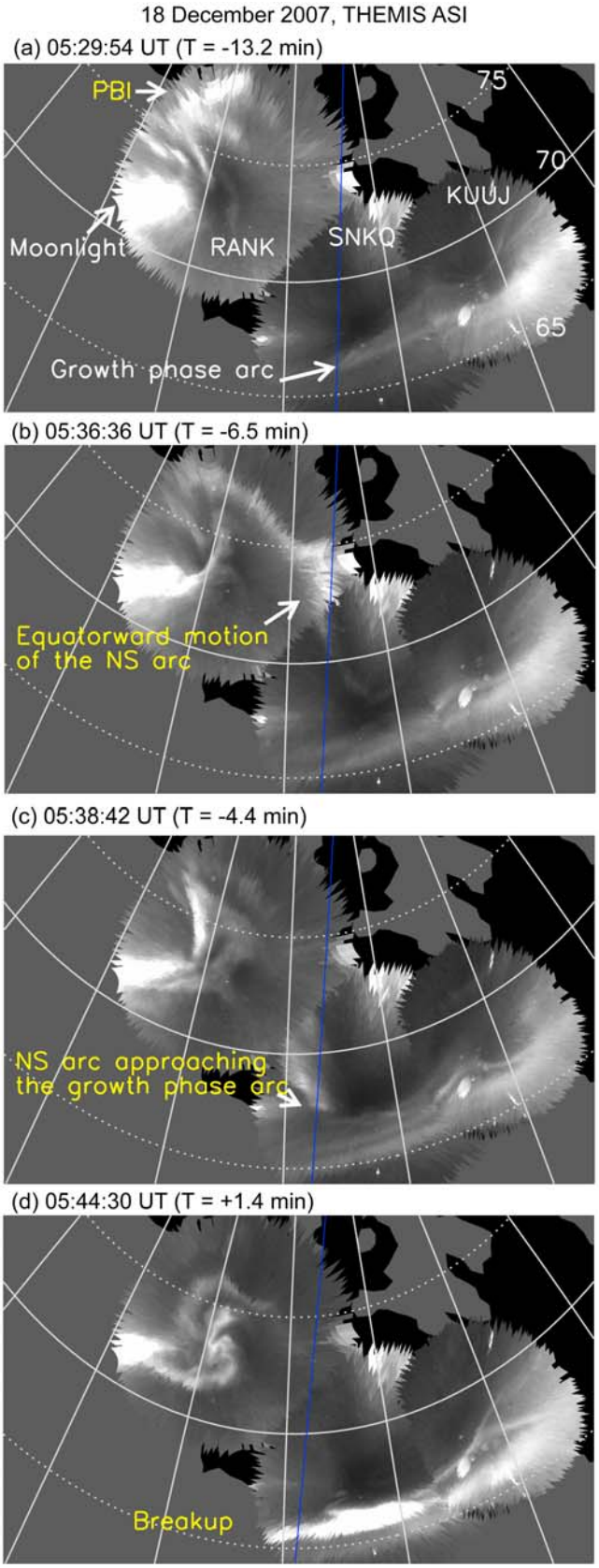

location along a pre-existing growth phase arc. Such two-dimensional evolution, which is common in our events, can lead to precursors being missed by meridian scanning photometers or imagers with limited FOVs.

2.3. The 18 December 2007 Auroral Breakup

[15] Figure 4 shows ASI data from three imagers near Hudson Bay during an auroral onset on 18 December 2007. The full sequence is shown in Movie S3. A growth phase arc is seen at ~67° MLAT prior to onset.

[16] A pre-onset auroral sequence similar to that for the event in Figure 3 is identified for this event. A PBI was detected at ~77° MLAT in the poleward portion of the RANK imager 10.8 min prior to the auroral onset (seen clearly in Figure 4a, which was taken 0.6 min after the PBI onset). An N-S arc initiated at the PBI, moved equatorward (Figure 4b), and reached the equatorward portion of the auroral oval ~1.5 min prior to onset (Figure 4c). Opposite to the event in Figure 3, the pre-onset aurora turned slightly eastward and crossed the magnetic midnight meridian. The onset then occurred to the east of the N-S arc at 05:43:06 UT, as seen in the 05:44:30 UT image in Figure 4d. As for the 4 February 2008 event, no auroral activity was detected just poleward of the center of the onset location, but the pre-onset auroral form reached the growth phase arc 0.6 MLT away from the onset location.

[17] The time evolution of the pre-onset auroral form can also be identified in keograms shown in Figures 1k–1o. Onset (second vertical line) is marked by substantial auroral intensification and poleward expansion within the SNKQ imager FOV (Figure 1n) and enhancement of the westward electrojet (Figure 1p). The equatorward motion of the N-S arc originated from the poleward boundary, as clearly identified in Figures 1l and 1m. After reaching the equatorward portion of the auroral oval, the auroral enhancement propagated eastward for a short time at ~64° MLAT, as seen by a weak intensification just prior to onset in Figure 1n. It had been geomagnetically quiet for 1.5 h before this PBI. There was weak preceding auroral activity ~3 h in MLT to the west at ATHA (Figure 1o), possibly associated with a N-S structure partially obscured by moonlight, but the activity ceased before the SNKQ onset. Another brightening occurred at ATHA at 05:39 UT, ~1 min after the SNKQ onset.

[18] The sequence of a PBI, the following equatorward motion of the N-S arc, and the arc motion toward the onset location just prior to onset, as seen in all of the three events, are repeatable auroral precursor onset signatures seen in most of the substorm events we examined. Furthermore, the pre-onset N-S and E-W arc motion seems to consistently follow the ionospheric two-cell convection pattern. On 4 February 2008, the PBI and N-S arc formed in the dusk

Figure 4. THEMIS ASI data for an auroral onset on 12 December 2007 auroral onset. The format is same as Figure 2. ASIs used are RANK, SNKQ (66.45° MLAT and 356.99° MLON) and KUUJ (66.89° MLAT and 13.23° MLON). Onset occurred at 05:43:06 UT. The entire sequence is shown in Movie S3.

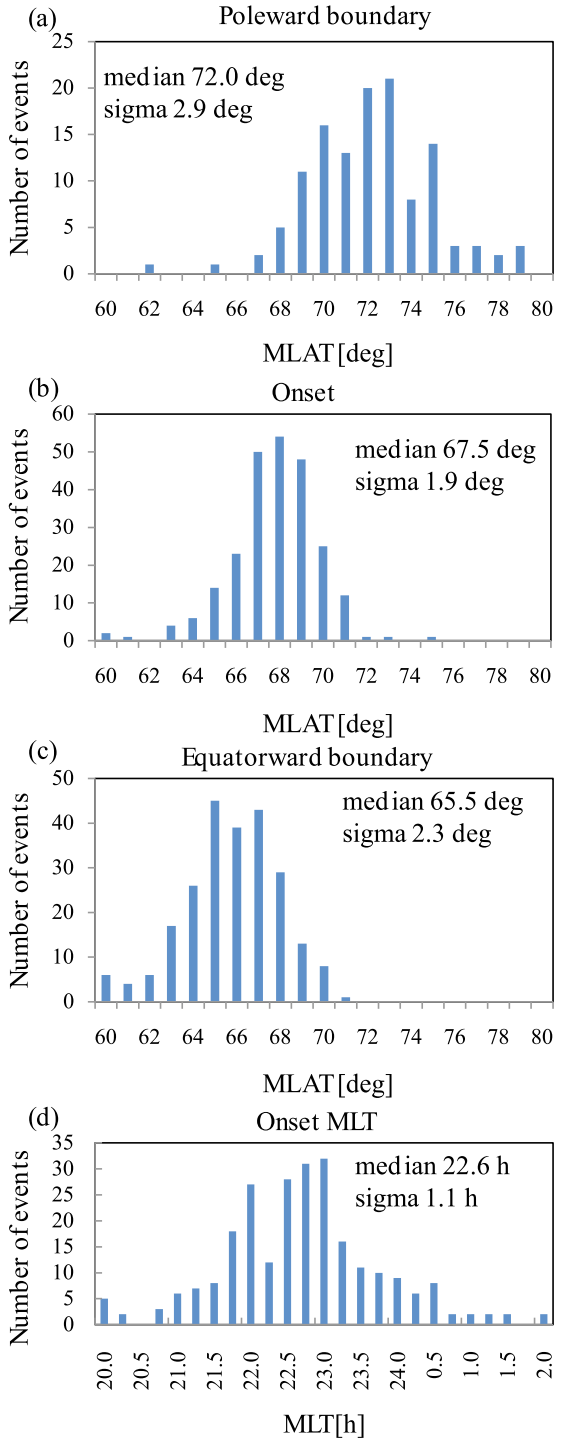

Figure 5. Distribution of the onset and oval boundary locations: (a–c) MLAT distributions of the poleward boundary, onset and equatorward boundary at onset time. (d) Distribution of onset MLT.

convection cell and moved equatorward and clockwise around the Harang flow shear approaching the pre-midnight onset location from east to west (Figure 3 and Movie S2). Conversely, on 18 December 2007, the pre-onset arc formed in the dawn cell and moved equatorward and eastward, i.e., counter-clockwise, toward a postmidnight onset location (Figure 4 and Movie S3).

3. Statistical Study

[19] In this section, we present statistics of the various time sequence features that we find lead to substorm onset. We selected 249 auroral onset events from November 2007 to April 2008 identified visually with the criterion that substantial auroral intensification occurred near the equatorward boundary of the auroral oval, the initial brightening being fully covered by the FOVs of any of the 20 ASIs. Onsets were identified visually, because it is not possible to select an intensity threshold under the variable sky conditions and viewing angles. We not only include both full poleward expansions (poleward motion lasting more than 3 min) and pseudo-breakups (poleward motion less than 3 min), but also present results of each separately when showing the occurrence of pre-onset aurora. The onset event list is provided as Data Set S1 in the auxiliary material.

3.1. MLAT and MLT Distribution

[20] Figure 5 shows distributions of auroral onset and oval locations. The poleward and equatorward boundaries are defined as poleward-most and equatorward-most luminosity edges at the onset MLT or at the MLT of N-S arc formation if such an arc is detected. Since white light imagers cannot distinguish proton and electron emissions, the equatorward boundary may include both of the components. However, proton aurora could affect the boundary location in the premidnight sector, since auroral spectral observations have shown that the proton auroral oval extends equatorward of the electron oval in the premidnight sector [*Eather and Mende*, 1971, 1972], as expected from particle drift in the presence of eastward corotation. Consistent with this, simultaneous observations with the NOAA POES spacecraft and with the PFISR radar have shown that enhanced *E* region ionization observed near the equatorward boundary of the oval corresponds to proton precipitation, particularly in the premidnight sector [*Donovan et al.*, 2008; *Zou et al.*, 2009b; *Lyons et al.*, 2010]. Locations of the onset and equatorward boundary were determined for all the 249 onset events, while the poleward boundary was identified only when the imager FOVs cover a wide latitude range up to ~75° MLAT (124 events, 50% of all events).

[21] MLAT distributions of each boundary approximately follow normal distributions with median latitudes and standard deviations indicated in Figures 5a–5c. As defined, the average onset location is close to (~2° poleward of) the average equatorward boundary of the auroral oval and ~4.5° equatorward of the average poleward boundary. The MLT distribution given in Figure 5d shows that onset tends to occur preferably in the premidnight sector. The median onset MLT, 22.6 h with a standard deviation of 1.1 h, is consistent with statistical studies performed using global auroral observations from space [*Frey et al.*, 2004; *Grocott et al.*, 2009]. The locations of the poleward and equatorward boundaries are consistent with the study by *Gjerloev et al.* [2008].

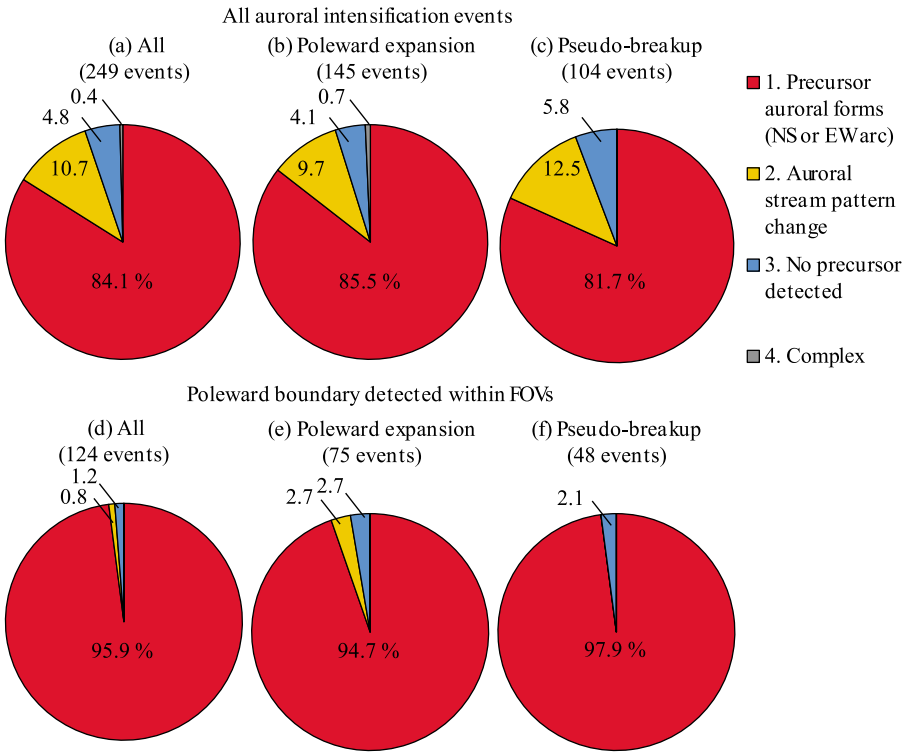

Figure 6. Occurrence rates of pre-onset auroral forms: (a) all of the events, (b) events where poleward expansion is detected after intensification, and (c) the remainder of the events (pseudo-breakup). (d)–(f) The same as Figures 6a–6c except for events where the poleward boundary is detected over ~1 MLT relative to onset MLT or to the MLT of N-S arc formation. See text for descriptions of each category.

3.2. Occurrence Probability of Pre-Onset Aurora

[22] To determine the occurrence frequency of auroral forms that are precursors for onset, we classified events into the following four categories: (1) A new N-S and/or E-W arc reaching the onset location just before an auroral onset is observed moving toward the onset location as for the cases shown in Section 2; (2) No newly formed N-S or E-W arc is seen moving toward the onset location, but the pre-existing growth phase arc exhibits structured forms moving along the arc. Note that a sudden (generally equatorward) shift in the location of the pre-existing arc is seen just before auroral onset; (3) No precursor activity except faint growth phase arcs is detected in available imager FOVs; and (4) other complex events. We first detected auroral onset using the criteria described above. Then we searched the region around the onset to see if there was any observable auroral form propagating toward the onset location. If enhanced brightness (N-S or E-W arcs) moving toward onset location was visually detected above the background, these were traced backward to the poleward boundary intensification, emerging point within the auroral oval, or the edge of FOVs. Thus any other auroral activity was removed and does not affect results of this study. Note that the background depends on the sky condition, so that weaker forms moving toward the onset location could be missed for some events.

[23] The occurrence probabilities of each category for all events are shown in Figure 6a. The majority (84.1%) of substorm onset events fall into the first category, showing that the sequence seen in the cases in Section 2 are repetitive. As shown below, pre-onset auroral forms in this category typically originated from auroral activity at or near the poleward boundary of the auroral oval. An N-S arc extends from the poleward boundary and reaches an onset location directly or after turning into an E-W arc. The second category contains most of the remaining events (10.7%). Sudden changes in auroral motion patterns, possibly related to changes in magnetospheric convection prior to onset, can thus also be a precursor of auroral onset. Because ASI coverage for these events was, in general, sparser than for the category 1 events, newly formed auroral forms could have preceded some category 2 events, as well. Category 3 events, for which no pre-onset auroral activity was detected (4.8%), include many in which bright moonlight or partly cloudy skies might have obscured faint auroral forms. Thus, it can be concluded that substorm auroral onset in the absence of a precursor is rare, and most auroral substorms are associated with pre-onset auroral forms moving toward the onset location.

[24] Figures 6b and 6c show occurrence probabilities using the same format as Figure 6a, except that they include only auroral intensification events with and without poleward expansion, respectively. Percentages in each category are essentially the same as those given in Figure 6a. Contact with pre-onset auroral forms is thus a common precursor for both poleward expansion and pseudo-breakup events. In order to increase statistical significance and because of the lack of significant differences in Figure 6, the following studies include both types of events.

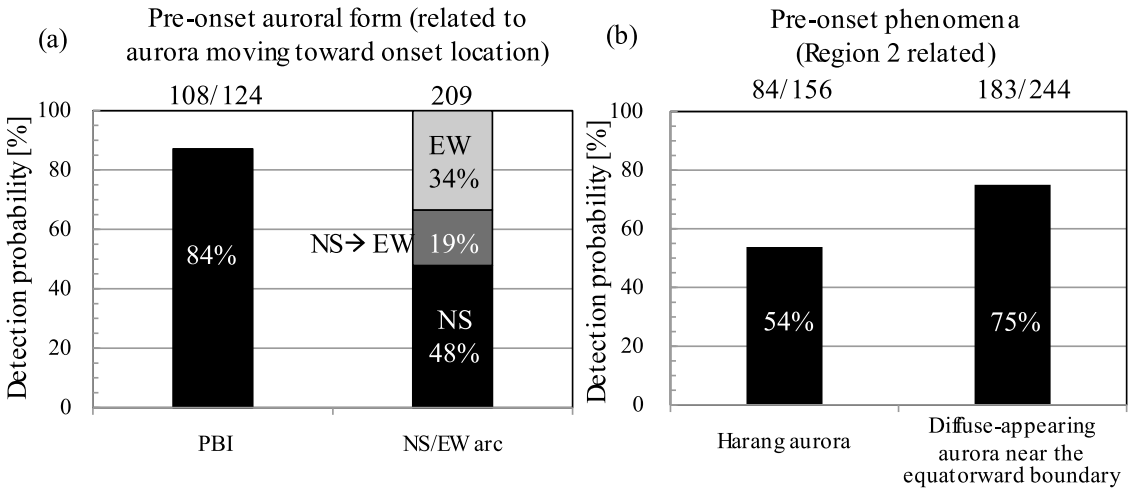

Figure 7. Occurrence rates of pre-onset phenomena: (a) pre-onset auroral forms related to those approaching onset locations just prior to onset, and (b) pre-onset phenomena related to region 2 FACs. Grey areas correspond where E-W arcs turned from N-S arcs approaching onset locations. Total number of events and number of events matching each condition are shown on the top of each area.

[25] As noted above, pre-onset N-S or E-W arcs could occur out of the available ASI FOVs when FOVs are limited to stations located only nearby the onset location. We thus selected events where FOVs either cover more than 1 MLT relative to the onset MLT or cover around the MLT of N-S arc formation if such an arc is detected. Figures 6d–6f shows the distribution of these events using the same format as Figures 6a–6c. Remarkably, pre-onset auroral forms were detected for almost all the events where FOVs had sufficient coverage. This result confirms that the onset time sequence described in the previous section is a feature of almost all substorms.

[26] Figure 7a presents detection probabilities of the different types of pre-onset auroral forms in category 1 (209 events). Existence of N-S or E-W arcs approaching the onset location was determined for all events. Here, N-S arcs occasionally turn into E-W arcs after reaching the equatorward portion of the auroral oval. PBI occurrence was obtained for all events where the FOVs of imagers covered at least 2 h of MLT of the poleward boundary centered on the MLT of the N-S arcs. For 84% of such events, a PBI was seen connected to the N-S arcs leading to onset. Thus, enhanced flows that brought newly supplied plasma across the open-closed boundary were a frequent precursor to onset. PBIs were followed by N-S arcs extending equatorward, and the N-S arcs were observed to directly reach the onset location for about half of the onset events (48%). For 19% of onset events, N-S arcs turned into E-W arcs, and the associated auroral enhancement approached the onset location by moving azimuthally along the pre-existing growth phase arc. For the remainder of the events (34%), E-W auroral enhancements come from outside the imager FOVs along growth phase arcs without detection of a PBI or N-S arc. Those events may also be connected to N-S arcs, but such arcs would have extended equatorward to the growth phase arc outside of the FOVs of the available ASIs. The high occurrence rate (53%) of E-W arcs as pre-onset aurora indicates that it is approximately as common for the plasma population leading to onset in the near-Earth plasma sheet to drift roughly azimuthally toward the onset locations as for onset to occur near the location where the plasma first reaches the equatorward portion of the auroral oval.

[27] Figure 7b shows detection probabilities of region 2-related auroral forms. Auroral forms rotating clockwise poleward of the onset location prior to onset (Harang aurora) were detected in 54% of the onset events where FOVs extended sufficiently both in latitude and longitude to detect motion of auroral forms. This category is shown separately from the N-S or E-W arcs since the Harang aurora exists continually prior to onset, though the auroral forms that reached the onset location generally rotated clockwise as well. Broad, diffuse-appearing, auroras near the equatorward boundary showed a high detection probability (75%), when FOVs covered the equatorward boundary of the auroral oval. Only 15% of events did not show evidence of either Harang or diffuse-appearing aurora.

[28] The high detection probabilities of Harang auroras and diffuse-appearing auroras indicate the existence of the Harang flow shear and high plasma pressure in the near-Earth plasma sheet prior to onset. Since these are basic features of the magnetosphere-ionosphere coupling of the region 2 FAC system, they indicate that a well-developed region 2 FACs in the duskside convection cell is a likely pre-condition for substorm onset in the pre-midnight sector.

3.3. Spatial and Temporal Evolution of Pre-Onset Aurora

[29] Next, we consider the time sequence of pre-onset auroras for all of the events in category 1 of Figure 6 in a way similar to that used for the case studies in Section 2. The time lag between initiation of PBIs and onsets is given in Figure 8a for events where PBIs were detected within FOVs, the median time lag and standard deviation being 5.5 and 4.9 min. A PBI is thus initiated typically 5.5 min prior to onset, followed by equatorward motion of an N-S arc extending from the poleward boundary. This time lag is

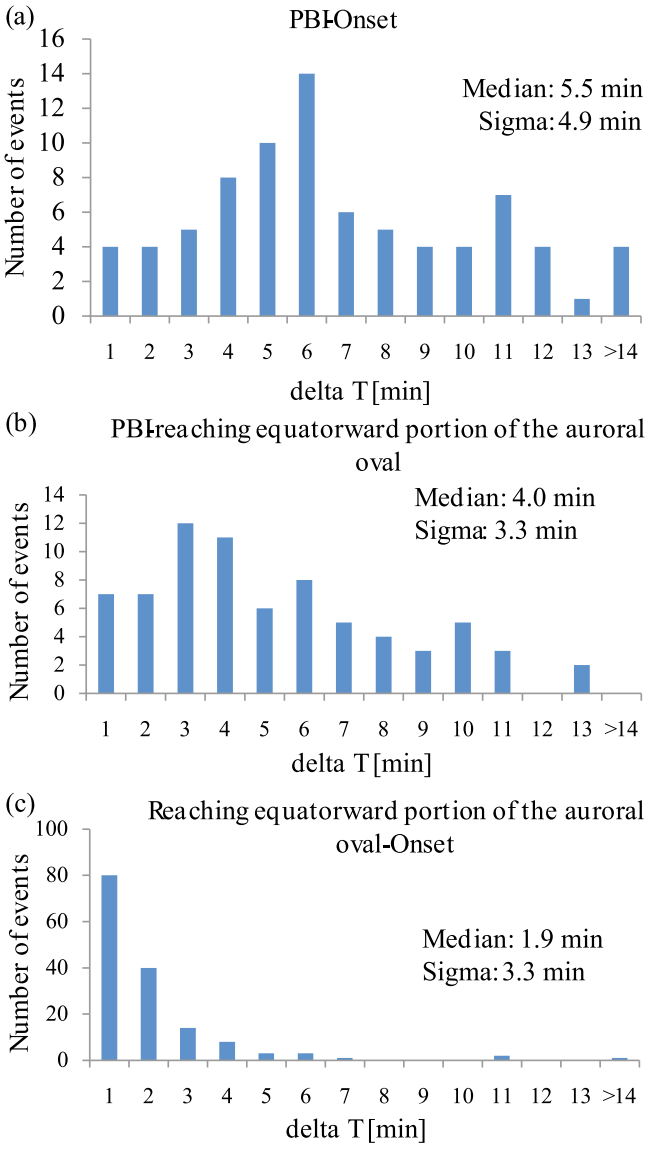

Figure 8. Time evolution of pre-onset auroral forms: time difference between (a) PBI and onset, (b) PBI and N-S arc reaching the equatorward portion of the auroral oval and onset, and (c) pre-onset arc reaching the equatorward portion of the auroral oval and onset.

much longer than the communication time for MHD waves from the mid-tail plasma sheet to the ionosphere (a few minutes) [*Chi et al.*, 2009].

[30] A wide spread of the time lag comes from variations in the oval width and the speed of the equatorward-motion of the N-S arc in different events. The MLAT separation between the poleward boundary and onset varied considerably, as indicated by the larger standard deviation of the location of the poleward boundary than that of onset MLAT in Figure 5. Also, the speed of the N-S arc can be different depending on the speed and tilt of plasma convection. To consider in more detail the motion of pre-onset arcs, their trajectories were divided into segments before and after N-S arcs reach the equatorward portion of the auroral oval. Time lags for each segment are shown in Figures 8b (events with PBIs and N-S arcs) and 8c (events with N-S arcs). A median time lag between initiation of PBIs and arrival of N-S arcs at the equatorward portion of the auroral oval of 4.0 min (Figure 8b) indicates the time interval to transport plasma from the open-closed field line to the onset latitude. Taking into account an averaged separation between the poleward boundary and onset latitude of 4.5° shown in Figure 5, the averaged equatorward speed of the N-S arc is 2.0 km/s. This speed is faster than indicated by radar observations of typical ionospheric plasma flows during PBIs shown by *de la Beaujardière et al.* [1994] during quiet periods (~500 m/s), but is near the highest speeds seen for the pre-onset flow enhancements in the companion paper [*Lyons et al.*, 2010]. It should also be remembered that the peak flow speeds may be quite short in duration, and thus not detectable with the 4 min cycle of the radar used in the above studies.

[31] The time lag between arrival of N-S arcs at the equatorward portion of the auroral oval and onset is shown in Figure 8c. The typical time lag of 1.9 min might correspond to the time-scale for instability growth in the near-Earth plasma sheet triggered by new plasma injections.

[32] Figure 9 shows the MLT evolution of pre-onset auroral forms. PBI MLT relative to onset MLT is given in Figure 9a for events with PBIs. PBIs tended to occur at later MLT than onset, indicating that pre-onset arcs extending from PBIs are formed near midnight and move duskward within the duskside convection cell. Auroral onsets then occurred in the premidnight sector centered at 22.6 MLT as shown in Figure 6d. The MLT differences corresponding to the time lags in Figures 8b and 8c are shown in Figures 9b (events with PBIs and N-S arcs) and 9c (events with N-S arcs). The PBI MLT is on average roughly the same as that of the N-S arc reaching the equatorward portion of the auroral oval (Figure 9b), indicating that an N-S arc started from a PBI moves around the Harang flow shear and reaches a growth phase arc at approximately the same longitude. Roughly half of the auroral intensifications occur near the meridian where the N-S arc reaches the equatorward portion of the auroral oval, while N-S arcs turn into E-W arcs and move ~1 MLT westward in most of the other events (Figure 9c).

[33] As shown in Figures 1, 4 and 9, pre-onset auroral forms do not necessarily extend along onset meridians but are often highly tilted in the azimuthal direction. Figure 10 quantifies the geometry of the growth phase arc and pre-onset aurora just before onset. Figure 10a shows the tilt angle distribution of growth phase arcs as a function of MLT. As shown in the schematic picture on the right, the azimuthal angle of the normal vector of the arc is measured clockwise from geomagnetic north. A small average and standard deviation of −0.8° and 6.5° indicates that the growth phase arc is almost aligned in the azimuthal direction just before onset.

[34] Figure 10b shows the attack angle distribution of pre-onset auroral forms just before their arrival at the equatorward portion of the auroral oval. The orientation of pre-onset auroral arcs is highly tilted from geomagnetic north. Over half of the arcs (64.0%) approach within 45° of geomagnetic east, indicating that onset locations are embedded deeply in the duskside convection cell. Pre-onset auroral

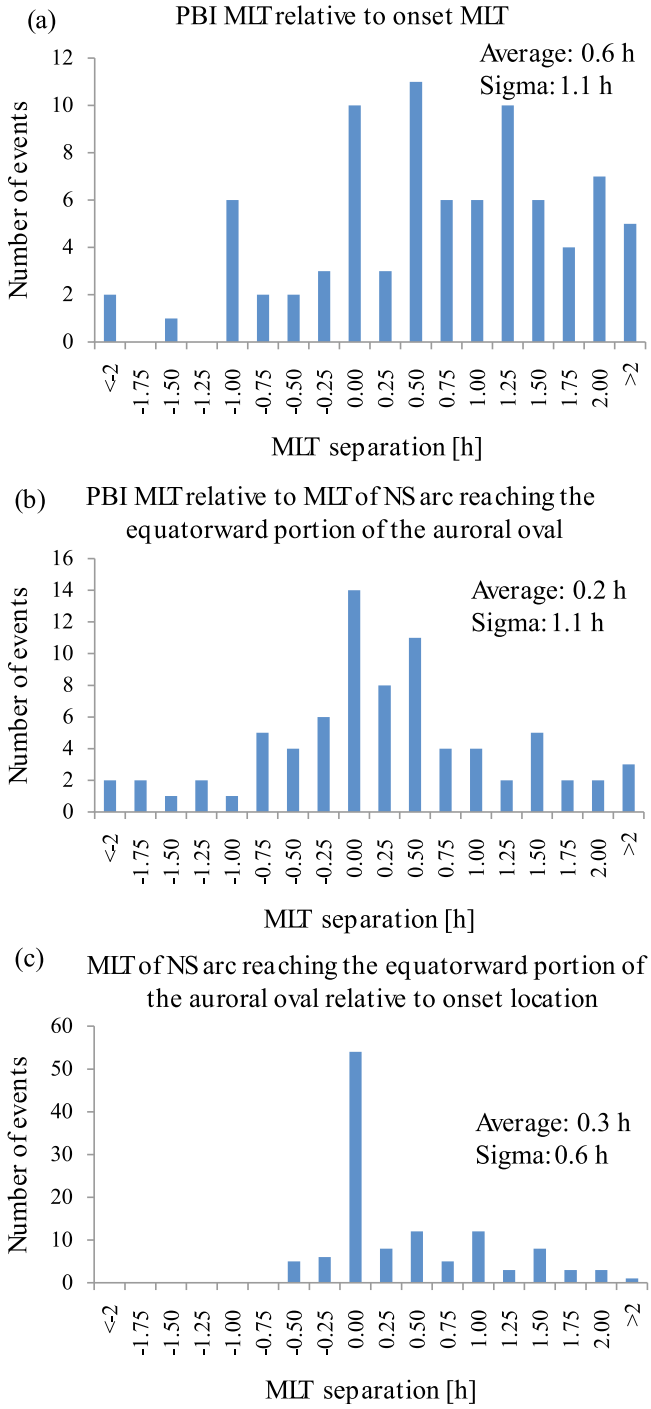

Figure 9. MLT evolution of pre-onset auroral forms: MLT difference between (a) PBI and onset, (b) PBI and N-S arc reaching the equatorward portion of the auroral oval, and (c) pre-onset arc approaching onset location.

forms reach within 45° of geomagnetic north for a smaller percentage (31.5%) of events. These results indicate that the plasma convection pattern has an important role in motion of pre-onset auroral forms, and the duskside convection cell where the region 2 current system is well developed is a favorable location for auroral onset. A small percentage (4.5%) of the pre-onset auroral forms reach the equatorward portion of the auroral oval from within 45° of magnetic west, leading to onsets within the dawn convection cell.

4. Conclusion

[35] The time sequence of auroral activity preceding most substorm onsets we have inferred from the event and statistical studies of observations from the THEMIS ground ASI array is summarized as follows and in Figure 11:

[36] 1. The initial feature of pre-onset auroral activity is a PBI, which starts ~5.5 min prior to onset.

[37] 2. An N-S arc extending from the PBI then moves equatorward, roughly following the preexisting flow pattern around the Harang flow shear.

[38] 3. The N-S arc reaches the equatorward portion of the auroral oval, where growth phase arcs or diffuse-appearing aurora are present, ~2 min prior to onset. About half of onset occurs at this location.

[39] 4. For about half the cases, the N-S arc turns into enhanced auroral brightness that moves azimuthally along the growth phase arc.

[40] 5. Onset occurs when the azimuthally moving enhanced auroral brightness reaches the onset location.

[41] Although each auroral feature in the above sequence is well known, the present study links these features together, giving evidence that a connection between the poleward and equatorward boundaries of the aurora oval leads to substorm onset.

[42] The azimuthal motion is most often directed westward, leading to onset west of the N-S arc, but an eastward motion is seen for ~5% of events. For the half of the events without discernible azimuthal motion of brightness along the growth phase arc, aurora onset occurs near the meridian where the N-S arc reaches the equatorward portion of the auroral oval. A high detection probability of pre-onset auroral forms moving toward the onset location (84% for all events, 96% when there is good ASI coverage) indicates that the above time sequence is common to most substorms. Furthermore, the high incidence of PBIs (84%) observed to initiate the sequence, together with the known relation between PBIs and N-S arcs and flow channels, leads to the inference that the pre-onset sequence starts with the enhanced transport of new plasma across the open-closed field line boundary. This enhanced transport corresponds to a localized enhancement of the reconnection rate, which would reflect an enhancement in reconnection preceding substorm onset as has been seen with the THEMIS spacecraft [*Angelopoulos et al.*, 2008]. This then leads to a channel of enhanced earthward flow carrying the new plasma earthward, which is manifested by the N-S arc seen moving equatorward. The high occurrence of N-S arcs indicates that equatorward motion of a pre-onset aurora inferred by *Oguti* [1973] and *Kepko et al.* [2009] for one event may be common, and the present study clarified that the pre-onset aurora initiates from a PBI.

[43] We have found that motion of the pre-onset auroral forms is related to the preexisting ionospheric convection pattern and is connected to the MLT location of onset. We frequently observe that the auroral forms leading to onset approach the onset location from the east or northeast. This suggests that the motion of the N-S aurora approximately follows the duskside convection cell, leading to pre-

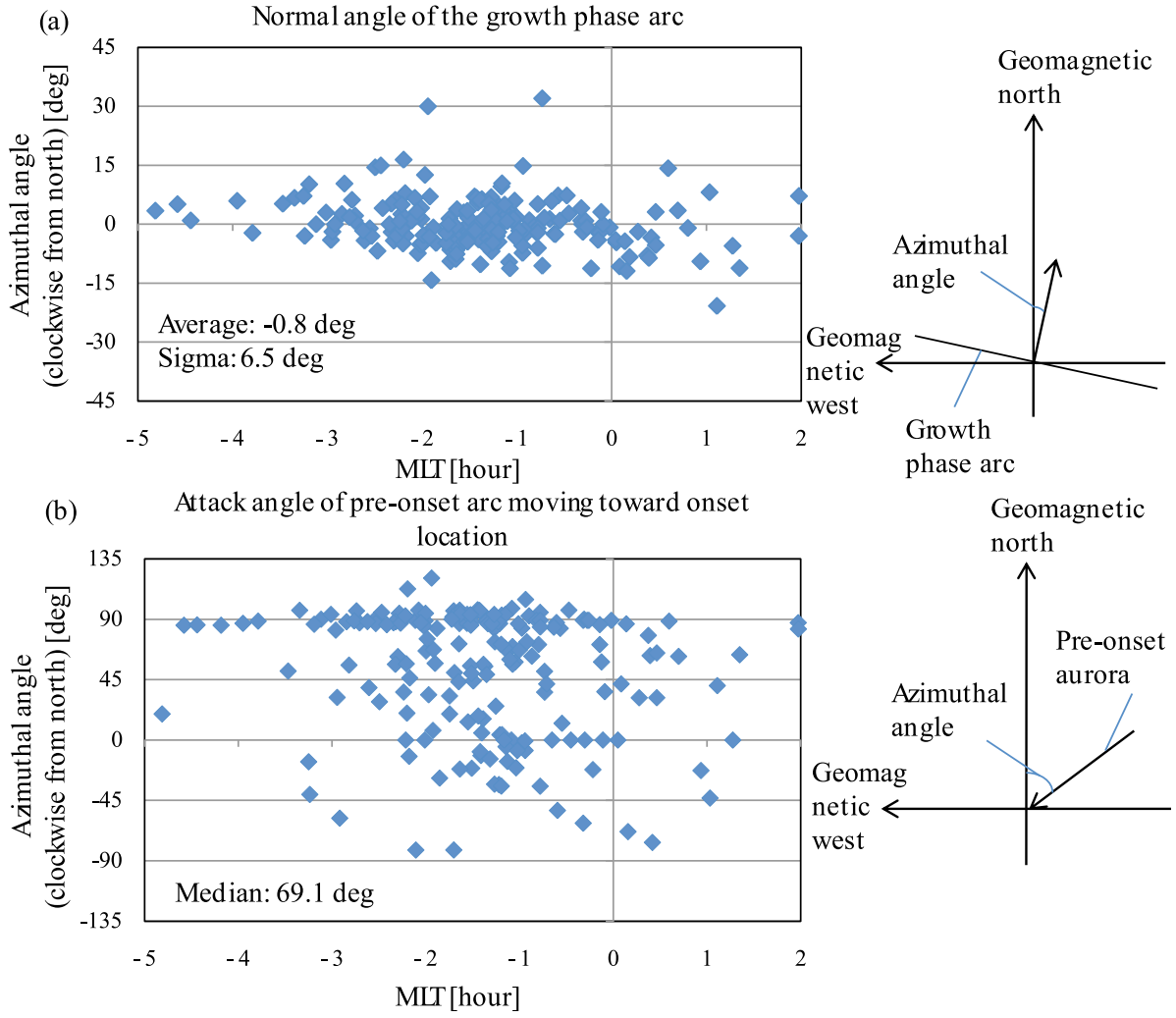

Figure 10. (a) Tilt angle of the growth phase arc. The normal angle of the growth phase arc is positive clockwise from geomagnetic north. (b) Orientation of pre-onset auroral arcs. The tangential angle of the pre-onset phase arc is positive clockwise from geomagnetic north.

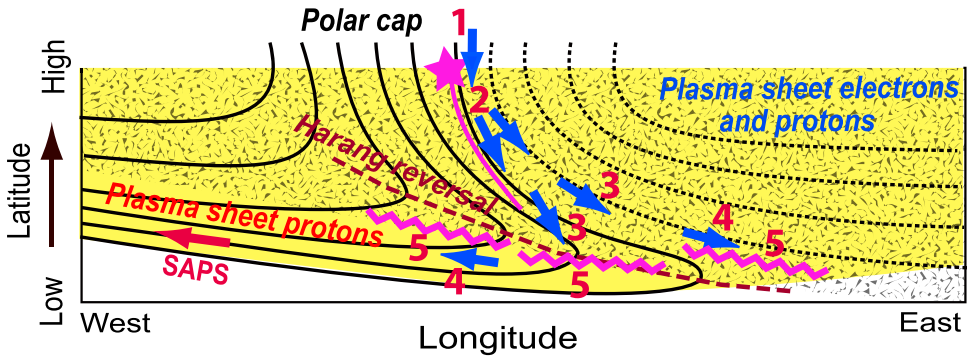

Figure 11. Schematic illustration of motion of pre-onset auroral forms and their relation to nightside ionospheric convection. The pink star, NS-oriented pink line, and azimuthally extended wavy lines indicate a PBI, NS-oriented arc and onset arcs, respectively. Blue arrows illustrate the plasma flow pattern inferred from pre-onset auroral motion. Numbers 1–5 show time evolution of pre-onset aurora (see text). Yellow and gray areas correspond to proton and electron precipitations.

midnight onsets as illustrated in Figure 11. Some N-S auroras follow the dawn convection cell, which generally lead to onsets located from near midnight to postmidnight as is also illustrated in Figure 11. The importance of the convection pattern is supported by a high detection probability of Harang aurora (54%), an auroral form that rotates clockwise just poleward of the onset latitude, and the pre-onset auroral forms move around the Harang aurora with the same sense of rotation. It is worth noting that the pre-onset auroral forms do not strictly follow the convection flow, which by itself has considerable time variations, and that magnetic drifts strongly affect the drift paths of particles as they reach the inner plasma sheet. Our observations indicate, however, that the convection pattern has a strong effect on the motion of the pre-onset auroral forms.

[44] The above time sequence gives evidence for the connection between auroral onset and the pre-onset aurora starting at the poleward boundary. Although the present study does not give in situ observations in the magnetosphere of a flow channel or onset instability, the temporal evolution of the pre-onset auroral form can be regarded as motion of magnetospheric plasma, based on the known association of PBIs and N-S arcs with flow bursts in the magnetotail. First, new plasma, presumably with lower entropy than the surrounding plasma [*Yang et al.*, 2008; *Wolf et al.*, 2009], is supplied across the open-closed field line boundary. This plasma is then transported earthward along an azimuthally narrow flow channel, with upward field-aligned currents and the N-S aurora measured by ASIs along its westward edge. While interchange motion is presumably responsible for the flow channel that brings the low-entropy plasma earthward, a separate instability, which might also be an interchange mode, is triggered near the inner edge of the electron plasma sheet by the intrusion of the new plasma. Auroral brightening could occur within the ionospheric footprint of this instability, followed by either a pseudo-breakup or full onset.

[45] Our observations also indicate the importance of the electrodynamic coupling associated with the region 2 current system, which is consistent with previous observations [*Zou et al.*, 2009a, 2009b]. In addition to the guiding of the pre-onset flows and resulting influence on the onset MLT, the Harang aurora and fast westward motion of pre-onset auroral forms along the growth phase arc reflect a well-developed region 2 FAC system within the duskside convection cell. Furthermore, the high probability of diffuse-appearing aurora near the onset latitude indicates the existence of high plasma pressure along these inner plasma sheet field lines, which would drive large region 2 currents. High pressure in the near-Earth plasma sheet will also provide a favorable condition for interchange instability following an injection of low entropy plasma to this region [*Yang et al.*, 2008]. Note also that the evidence indicating that the equatorward portion of the growth phase arc may be the region of proton aurora and SAPS [*Lyons et al.*, 2009; *Zou et al.*, 2009a, 2009b] also implies connection with the region 2 system.

[46] In the companion paper [*Lyons et al.*, 2010], we use observations from the Sondrestrom incoherent scatter radar, located near the typical location of the nightside open-closed field line boundary, and from the Poker Flat incoherent scatter radar, located in the equatorward portion of the auroral oval. We show that a plasma flow enhancement, likely associated with PBIs, is commonly observed at a time preceding onset that is consistent with what we find in the present paper from the ASI observations. We also find a pre-onset flow increase shortly before substorm onset near the onset location using ISR [*Lyons et al.*, 2010] and SuperDARN radars (S. Zou, personal communication, 2009). These radar observations thus support the above suggestion that an influx of new plasma crossing the nightside separatrix and intruding to the near-Earth magnetosphere along channels of enhanced flow leads to substorm onset. It is highly desirable to test this idea using in situ spacecraft observations within the plasma sheet during conjunctions with the aurora forms that lead to onset. Such a study is currently in progress using THEMIS spacecraft observations (X. Xing, personal communication, 2009).

[47] **Acknowledgments.** This work was supported by National Science Foundation grants ATM-0646233 and ATM-0639312, NASA grant NNX07AF66, NASA contract NAS5-02099, and JSPS Research Fellowships for Young Scientists. Deployment of the THEMIS ASIs was partly supported by CSA contract 9F007-046101. Alaska magnetometer data were obtained from Geophysical Institute of University of Alaska, Fairbanks.

[48] Bob Lysak thanks the reviewers for their assistance in evaluating this paper.

References

Akasofu, S.-I. (1964), The development of the auroral substorm, *Planet. Space Sci.*, *12*, 273–282, doi:10.1016/0032-0633(64)90151-5.

Akasofu, S.-I. (2004), Several 'controversial' issues on substorms, *Space Sci. Rev.*, *113*, 1–40, doi:10.1023/B:SPAC.0000042938.57710.fb.

Angelopoulos, V. (2008), First results from the THEMIS Mission, *Space Sci. Rev.*, *141*(1–4), 453–476, doi:10.1007/s11214-008-9378-4.

Angelopoulos, V., et al. (2008), Tail reconnection triggering substorm onset, *Science*, *321*, 931, doi:10.1126/science.1160495.

Baumjohann, W., R. J. Pellinen, H. J. Opgenoorth, and E. Nielsen (1981), Joint two-dimensional observations of ground magnetic and ionospheric electric fields associated with auroral zone currents - Current systems associated with local auroral break-ups, *Planet. Space Sci.*, *29*, 431–447, doi:10.1016/0032-0633(81)90087-8.

Birn, J., M. Hesse, G. Haerendel, W. Baumjohann, and K. Shiokawa (1999), Flow braking and the substorm current wedge, *J. Geophys. Res.*, *104*, 19,895–19,903, doi:10.1029/1999JA900173.

Bristow, W. A., G. J. Sofko, H. C. Stenbaek-Nielsen, S. Wei, D. Lummerzheim, and A. Otto (2003), Detailed analysis of substorm observations using SuperDARN, UVI, ground-based magnetometers, and all-sky imagers, *J. Geophys. Res.*, *108*(A3), 1124, doi:10.1029/2002JA009242.

Chi, P. J., C. T. Russell, and S. Ohtani (2009), Substorm onset timing via traveltime magnetoseismology, *Geophys. Res. Lett.*, *36*, L08107, doi:10.1029/2008GL036574.

de la Beaujardière, O., L. R. Lyons, J. M. Ruohoniemi, E. Friis-Christensen, C. Danielsen, F. J. Rich, and P. T. Newell (1994), Quiet-time intensifications along the poleward auroral boundary near midnight, *J. Geophys. Res.*, *99*, 287–298, doi:10.1029/93JA01947.

Donovan, E., et al. (2008), Simultaneous THEMIS in situ and auroral observations of a small substorm, *Geophys. Res. Lett.*, *35*, L17S18, doi:10.1029/2008GL033794.

Eather, R., and S. Mende (1971), Airborne observations of auroral precipitation patterns, *J. Geophys. Res.*, *76*, 1746–1755, doi:10.1029/JA076i007p01746.

Eather, R., and S. Mende (1972), Systematics in aurora energy spectra, *J. Geophys. Res.*, *77*, 660–673, doi:10.1029/JA077i004p00660.

Elphinstone, R. D., et al. (1995), Observations in the vicinity of substorm onset: Implications for the substrom process, *J. Geophys. Res.*, *100*, 7937–7969, doi:10.1029/94JA02938.

Erickson, G. M., R. W. Spiro, and R. A. Wolf (1991), The physics of the Harang discontinuity, *J. Geophys. Res.*, *96*, 1633–1645, doi:10.1029/90JA02344.

Frey, H. U., G. Haerendel, S. B. Mende, W. T. Forrester, T. J. Immel, and N. Østgaard (2004), Subauroral morning proton spots (SAMPS) as a

result of plasmapause-ring-current interaction, *J. Geophys. Res.*, *109*, A10305, doi:10.1029/2004JA010516.

Gjerloev, J., R. Hoffman, J. Sigwarth, L. Frank, and J. Baker (2008), Typical auroral substorm: A bifurcated oval, *J. Geophys. Res.*, *113*, A03211, doi:10.1029/2007JA012431.

Gkioulidou, M., C.-P. Wang, L. R. Lyons, and R. A. Wolf (2009), Formation of the Harang reversal and its dependence on plasma sheet conditions: Rice convection model simulations, *J. Geophys. Res.*, *114*, A07204, doi:10.1029/2008JA013955.

Grocott, A., J. A. Wild, S. E. Milan, and T. K. Yeoman (2009), Superposed epoch analysis of the ionospheric convection evolution during substorms: Onset latitude dependence, *Ann. Geophys.*, *27*, 591–600, doi:10.5194/angeo-27-591-2009.

Henderson, M. G., L. Kepko, H. E. Spence, M. Connors, J. B. Sigwart, L. A. Frank, H. J. Singer, and K. Yumoto (2002), The evolution of north-south aligned auroral forms into auroral torch structures: The generation of omega bands and ps6 pulsations via flow bursts, in *Sixth International Conference on Substorms*, edited by R. M. Winglee, pp. 169–174, Univ. of Wash., Seattle, Wash.

Kepko, L., E. Spanswick, V. Angelopoulos, E. Donovan, J. McFadden, K.-H. Glassmeier, J. Raeder, and H. J. Singer (2009), Equatorward moving auroral signatures of a flow burst observed prior to auroral onset, *Geophys. Res. Lett.*, *36*, L24104, doi:10.1029/2009GL041476.

Lin, N., H. Frey, S. Mende, F. Mozer, R. Lysak, Y. Song, and V. Angelopoulos (2009), Statistical study of substorm timing sequence, *J. Geophys. Res.*, *114*, A12204, doi:10.1029/2009JA014381.

Lui, A. (1991), A synthesis of magnetospheric substorm models, *J. Geophys. Res.*, *96*, 1849–1856, doi:10.1029/90JA02430.

Lui, A., and J. Burrows (1978), On the location of auroral arcs near substorm onsets, *J. Geophys. Res.*, *83*, 3342–3348, doi:10.1029/JA083iA07p03342.

Lyons, L. R., T. Nagai, G. T. Blanchard, J. C. Samson, T. Yamamoto, T. Mukai, A. Nishida, and S. Kokobun (1999), Association between Geotail plasma flows and auroral poleward boundary intensifications observed by CANOPUS photometers, *J. Geophys. Res.*, *104*, 4485–4500, doi:10.1029/1998JA900140.

Lyons, L., C.-P. Wang, M. Gkioulidou, and S. Zou (2009), Connections between plasma sheet transport, Region 2 currents, and entropy changes associated with convection, steady magnetospheric convection periods, and substorms, *J. Geophys. Res.*, *114*, A00D01, doi:10.1029/2008JA013743.

Lyons, L., Y. Nishimura, Y. Shi, H.-J. Kim, S. Zou, C. Heinselman, M. Nicolls, and V. Angelopoulos (2010), Substorm triggering by new plasma intrusion: Incoherent-scatter radar observations, *J. Geophys. Res.*, *115*(A7), A07223, doi:10.1029/2009JA015168.

McPherron, R. L. (1979), Magnetospheric substorms, *Rev. Geophys.*, *17*, 657–681, doi:10.1029/RG017i004p00657.

Mende, S. B., S. E. Harris, H. U. Frey, V. Angelopoulos, C. T. Russell, E. Donovan, B. Jackel, M. Greffen, and L. M. Peticolas (2008), The THEMIS array of ground-based observatories for the study of auroral substorms, *Space Sci. Rev.*, *141*, 357–387, doi:10.1007/s11214-008-9380-x.

Miyashita, Y., et al. (2009), A state-of-the-art picture of substorm-associated evolution of the near-Earth magnetotail obtained from superposed epoch analysis, *J. Geophys. Res.*, *114*, A01211, doi:10.1029/2008JA013225.

Nakamura, R., W. Baumjohann, R. Schödel, M. Brittnacher, V. A. Sergeev, M. Kubyshkina, T. Mukai, and K. Liou (2001), Earthward flow bursts, auroral streamers, and small expansions, *J. Geophys. Res.*, *106*, 10,791–10,802, doi:10.1029/2000JA000306.

Oguti, T. (1973), Hydrogen emission and electron aurora at the onset of the auroral breakup, *J. Geophys. Res.*, *78*, 7543–7547, doi:10.1029/JA078i031p07543.

Rostoker, G., S.-I. Akasofu, J. Foster, R. A. Greenwald, A. T. Y. Lui, Y. Kamide, K. Kawasaki, R. L. McPherron, and C. T. Russell (1980), Magnetospheric substorms—Definition and signatures, *J. Geophys. Res.*, *85*, 1663–1668, doi:10.1029/JA085iA04p01663.

Rostoker, G., A. T. Y. Lui, C. D. Anger, and J. S. Murphree (1987), North–south structures in the midnight sector auroras as viewed by the Viking imager, *Geophys. Res. Lett.*, *14*, 407–410, doi:10.1029/GL014i004p00407.

Roux, A., S. Perraut, P. Robert, A. Morane, A. Pedersen, A. Korth, G. Kremser, B. Aparicio, D. Rodgers, and R. Pellinen (1991), Plasma sheet instability related to the westward traveling surge, *J. Geophys. Res.*, *96*, 17,697–17,714, doi:10.1029/91JA01106.

Samson, J. C., L. R. Lyons, P. T. Newell, F. Creutzberg, and B. Xu (1992), Proton aurora and substorm intensifications, *Geophys. Res. Lett.*, *19*, 2167–2170, doi:10.1029/92GL02184.

Sergeev, V. A., K. Liou, C.-I. Meng, P. T. Newell, M. Brittnacher, G. Parks, and G. D. Reeves (1999), Development of auroral streamers in association with localized impulsive injections to the inner magnetotail, *Geophys. Res. Lett.*, *26*, 417–420, doi:10.1029/1998GL900311.

Sergeev, V. A., et al. (2000), Multiple-spacecraft observation of a narrow transient plasma jet in the Earth's plasma sheet, *Geophys. Res. Lett.*, *27*, 851–854, doi:10.1029/1999GL010729.

Wolf, R. A., Y. Wan, X. Xing, J.-C. Zhang, and S. Sazykin (2009), Entropy and plasma sheet transport, *J. Geophys. Res.*, *114*, A00D05, doi:10.1029/2009JA014044.

Yang, J., F. R. Toffoletto, R. A. Wolf, S. Sazykin, R. W. Spiro, P. C. Brandt, M. G. Henderson, and H. U. Frey (2008), Rice Convection Model simulation of the 18 April 2002 sawtooth event and evidence for interchange instability, *J. Geophys. Res.*, *113*, A11214, doi:10.1029/2008JA013635.

Zesta, E., E. Donovan, L. Lyons, G. Enno, J. S. Murphree, and L. Cogger (2002), Two-dimensional structure of auroral poleward boundary intensifications, *J. Geophys. Res.*, *107*(A11), 1350, doi:10.1029/2001JA000260.

Zou, S., L. R. Lyons, C.-P. Wang, A. Boudouridis, J. M. Ruohoniemi, P. C. Anderson, P. L. Dyson, and J. C. Devlin (2009a), On the coupling between the Harang reversal evolution and substorm dynamics: A synthesis of SuperDARN, DMSP, and IMAGE observations, *J. Geophys. Res.*, *114*, A01205, doi:10.1029/2008JA013449.

Zou, S., L. R. Lyons, M. J. Nicolls, C. J. Heinselman, and S. B. Mende (2009b), Nightside ionospheric electrodynamics associated with substorms: PFISR and THEMIS ASI observations, *J. Geophys. Res.*, *114*, A12301, doi:10.1029/2009JA014259.

V. Angelopoulos, Institute of Geophysics and Planetary Physics, University of California, Los Angeles, 3845 Slichter Hall, Los Angeles, CA 90095, USA.

L. Lyons, Y. Nishimura, and S. Zou, Department of Atmospheric and Oceanic Sciences, University of California, Los Angeles, 405 Hilgard Ave., Los Angeles, CA 90095-1565, USA. (toshi@atmos.ucla.edu)

S. Mende, Space Sciences Laboratory, University of California, 7 Gauss Way, Berkeley, CA 94720, USA.